Purdue University
Purdue e-Pubs

International Refrigeration and Air Conditioning Conference

School of Mechanical Engineering

2016

A Helmholtz Energy Equation of State for Trifluoroethylene (R-1123)

Ryo Akasaka
Kyushu Sangyo University, Japan, ryo-a@ip.kyusan-u.ac.jp

Masato Fukushima
ASAHI GLASS CO., LTD., Japan, masato-fukusima@agc.com

Eric W. Lemmon
National Institute of Standa, eric.lemmon@nist.gov

Follow this and additional works at: http://docs.lib.purdue.edu/iracc

Akasaka, Ryo; Fukushima, Masato; and Lemmon, Eric W., "A Helmholtz Energy Equation of State for Trifluoroethylene (R-1123)" (2016). *International Refrigeration and Air Conditioning Conference.* Paper 1698.
http://docs.lib.purdue.edu/iracc/1698

This document has been made available through Purdue e-Pubs, a service of the Purdue University Libraries. Please contact epubs@purdue.edu for additional information.
Complete proceedings may be acquired in print and on CD-ROM directly from the Ray W. Herrick Laboratories at https://engineering.purdue.edu/Herrick/Events/orderlit.html

A Helmholtz Energy Equation of State for Trifluoroethylene (R-1123)

Ryo AKASAKA[1*], Masato FUKUSHIMA[2], Eric W. LEMMON[3]

[1] Department of Mechanical Engineering, Faculty of Engineering, Kyushu Sangyo University,
2-3-1 Matsukadai, Higashi-ku, Fukuoka 8138503, Japan
e-mail: ryo-a@ip.kyusan-u.ac.jp

[2] AGC Chemicals, Research & Development Division, ASAHI GLASS CO., LTD.,
10 Goikaigan, Ichihara 2908566, Japan
e-mail: masato-fukusima@agc.com

[3] Applied Chemicals and Materials Division, National Institute of Standards and Technology,
325 Broadway, Boulder, Colorado 80305, USA
e-mail: eric.lemmon@nist.gov

* Corresponding Author

ABSTRACT

A first fundamental equation of state explicit in the Helmholtz energy is presented for trifluoroethylene (R-1123). The independent variables of the equation of state are temperature and density. Following recent trends in the development of accurate equations of state, a functional form that includes Gaussian bell-shaped terms is optimized with the use of nonlinear least-squares fitting to the experimental data. The equation is valid for temperatures from 250 K to 480 K and for pressures up to 10 MPa. Typical uncertainties over the range of validity are 0.1 % for vapor pressures, 0.2 % for liquid densities, and 1 % for vapor densities, except in the critical region where larger deviations up to about 2 % are observed in densities. At temperatures below 300 K, deviations in vapor pressures are larger due to insufficient amount of experimental data. The equation shows reasonable extrapolation behavior in regions away from the experimental data.

1. INTRODUCTION

Much attention has recently been given to trifluoroethylene (R-1123) (CAS number 359-11-5) and its mixtures due to its preferable characteristics for working fluids in residential air conditioners. In particular, the mixtures of R-1123 with difluoromethane (R-32) are promising, because the mixtures exhibit azeotropic-like behavior. Refrigeration industry considers R-32/1123 mixtures as one possible alternative for R-410A, and research and development of air conditioners with the mixtures has started with some manufacturers. At this time, however, an appropriate method is still not provided for property calculations for the mixtures, and a thermodynamic property model with sufficient accuracies are strongly desired.

The objective of our project is the development of a reliable property model for R-32/1123 mixtures. Such property models generally require accurate pure-fluid equations of state. Since property information on R-1123 was very limited, we first performed experimental measurements of the critical parameters (Higashi and Akasaka, 2016), saturation properties (Fukushima et al., 2015; Kayukawa et al., 2015; Higashi and Akasaka, 2016), $p\varrho T$ relation (Fukushima et al., 2015; Kayukawa et al., 2015; Higashi and Akasaka, 2016; Kayukawa, 2016), and sound speeds in the vapor phase (Kano et al., 2016). In this work, a Helmholtz energy equation of state is formulated based on these measurements. The fundamental constants of R-1123 are given in Table 1, as well as the normal boiling-point temperature and acentric factor calculated from the equation of state developed in this work.

Table 1: Fundamental constants of R-1123

Property	Symbol	Value	Author
Molar mass	M	82.02455 g mol^{-1}	
Universal gas constant	R	8.3144621 J mol^{-1} K^{-1}	Mohr et al. (2012)
Critical temperature	T_c	331.80 K	Fukushima et al. (2015)
		331.73 K†	Higashi and Akasaka (2016)
Critical pressure	p_c	4.545 MPa	Fukushima et al. (2015)
		4.546 MPa†	Higashi and Akasaka (2016)
Critical density	ϱ_c	510 kg m^{-3}	Fukushima et al. (2015)
		504 kg m^{-3}	Higashi and Akasaka (2016)
		6.000 mol dm$^{-3\dagger}$	This work
		(492 kg m^{-3})	
Normal boiling point	T_b	214.06 K	This work
Acentric factor	ω	0.26134	This work

†Data used in this work

2. EXPERIMENTAL DATA

Tables 2 and 3 summarize the available experimental data for R-1123. The tables also present the absolute average deviations (AADs) from calculated values with the equation of state. The AAD in any property X is defined as

$$\mathrm{AAD}_X = \frac{100}{N_{\mathrm{exp}}} \sum_{i=1}^{N_{\mathrm{exp}}} \left| \frac{X_{\mathrm{exp}} - X_{\mathrm{calc}}}{X_{\mathrm{exp}}} \right|_i , \tag{1}$$

where N_{exp} is the number of data points for X, and the subscripts exp and calc indicate experimental and calculated values for X, respectively. Figure 1 shows the distribution of the $p\varrho T$ data.

3. EQUATION OF STATE

The equation of state is formulated with the Helmholtz energy as the fundamental property with independent variables of temperature and density. The form of the equation is

$$\frac{a(T,\varrho)}{RT} = \alpha(\tau,\delta) = \alpha^{\circ}(\tau,\delta) + \alpha^{\mathrm{r}}(\tau,\delta), \tag{2}$$

where a is the molar Helmholtz energy, α is the dimensionless Helmholtz energy, $R = 8.3144621$ J mol^{-1} K^{-1} (Mohr et al., 2012) is the universal gas constant, $\tau = T_c/T$ is the inverse reduced temperature, and $\delta = \varrho/\varrho_c$ is the reduced density. The dimensionless Helmholtz energy α is split into an ideal-gas part α° representing ideal-gas properties and a residual part α^{r} corresponding to the influence of intermolecular forces.

3.1 Ideal-gas Helmholtz energy

The dimensionless ideal-gas Helmholtz energy α° can be expressed as

$$\alpha^{\circ}(\tau,\delta) = \frac{a^{\circ}(T,\varrho)}{RT} = \frac{h_0^{\circ}\tau}{RT_c} - \frac{s_0^{\circ}}{R} - 1 + \ln\frac{\delta\tau_0}{\delta_0\tau} - \frac{\tau}{R}\int_{\tau_0}^{\tau}\frac{c_p^{\circ}}{\tau^2}\,d\tau + \frac{1}{R}\int_{\tau_0}^{\tau}\frac{c_p^{\circ}}{\tau}\,d\tau, \tag{3}$$

where c_p° is the ideal-gas isobaric heat capacity, $\tau_0 = T_c/T_0$, $\delta_0 = \varrho_0/\varrho_c$, T_0 is the temperature at a reference state, and ϱ_0 is the ideal-gas density at the reference state. This work sets the reference temperature T_0 and pressure p_0 to 273.15 K and 1.0 kPa, and therefore ϱ_0 is calculated as $\varrho_0 = p_0/(RT_0) = 4.4032 \times 10^{-4}$ mol dm^{-3}.

This work uses the following c_p° equation:

$$\frac{c_p^{\circ}}{R} = v_0 + \sum_{i=1}^{2} v_i \left(\frac{u_i}{T}\right)^2 \frac{\exp(u_i/T)}{[\exp(u_i/T) - 1]^2}, \tag{4}$$

Table 2: Experimental data for the saturation properties of R-1123

Author	No. of data (used)	Range T (K)	AAD (%)
Vapor pressures			
Fukushima et al. (2015)	16	313–331	0.58
Kayukawa et al. (2015)	20	260–324	1.56
Higashi and Akasaka (2016)	14 (14)	300–331	0.03
Raabe (2016)†	7 (7)	230–300	1.14
Saturated liquid densities			
Fukushima et al. (2015)	7 (6)	262–324	0.24
Fukushima et al. (2015) (Critical region)	5	329–331	1.56
Higashi and Akasaka (2016)	6 (6)	316–331	0.53
Raabe (2016)†	7	230–300	0.65
Saturated vapor densities			
Fukushima et al. (2015) (Critical region)	4	330–331	1.44
Higashi and Akasaka (2016)	10 (10)	322–331	2.63
Raabe (2016)†	7	230–300	3.65

†Determined with molecular simulation

Table 3: Experimental data for the single-phase properties of R-1123

Author	No. of data (used)	Range T (K)	Range p (MPa)	AAD (%)
$p\varrho T$ data (density)				
Fukushima et al. (2015)	69	313–473	1.39–9.72	2.16
Kayukawa et al. (2015)	57 (37)	259–400	0.20–4.15	0.58
Higashi and Akasaka (2016)	67 (66)	310–430	2.25–6.86	0.15
Kayukawa (2016)	33 (13)	261–340	1.00–7.00	0.77
Sound speeds				
Kano et al. (2016)	36 (12)	263–313	0.05–0.45	0.02

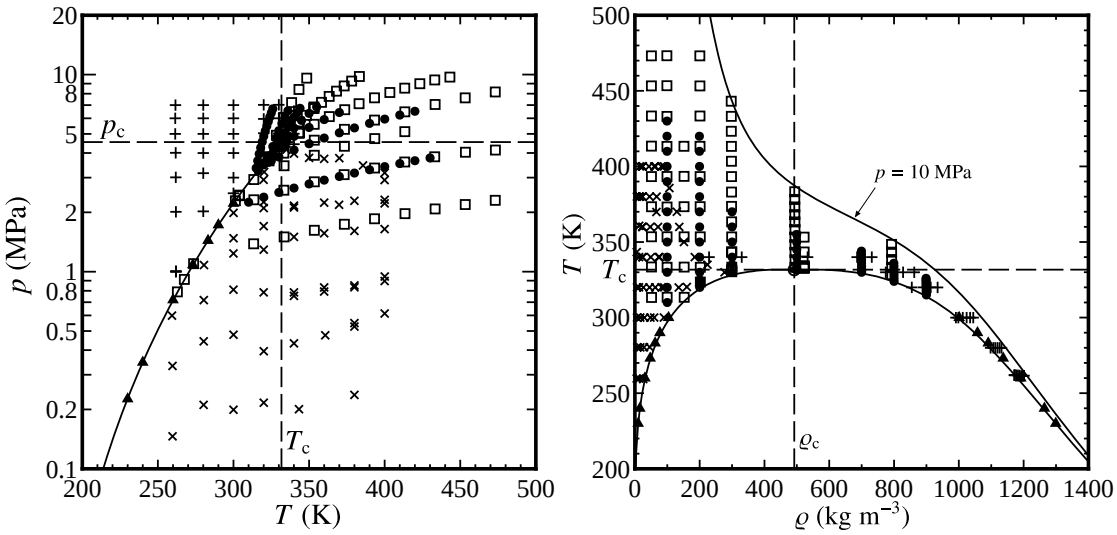

Figure 1: Distribution of experimental $p\varrho T$ data in the single phase region: (□) Fukushima et al. (2015), (×) Kayukawa et al. (2015), (•) Higashi and Akasaka (2016), (▲) Raabe (2016), (+) Kayukawa (2016).

where v_0 = 3.0, v_1 = 5.39533, v_2 = 7.79874, u_1 = 453 K, and u_2 = 1712 K. These coefficients were obtained from fitting the experimental c_p° data by Kano et al. (2016). Figure 2 shows the experimental data and calculated values from Eq. (4). For comparison, this figure also presents estimated values with Joback's method (Joback and Reid, 1987).

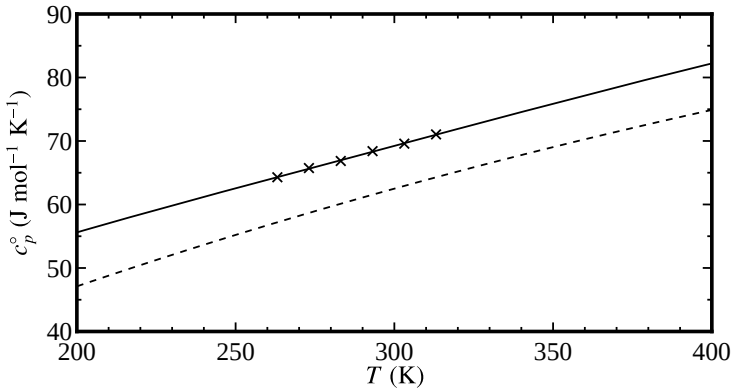

Figure 2: Ideal-gas isobaric heat capacity of R-1123: (×) Kano et al. (2016), (—) Eq. (4), (- - -) Joback's method (Joback and Reid, 1987)

3.2 Residual Helmholtz energy

In recent developments of accurate equations of state, the residual Helmholtz energy is often represented with the following functional form:

$$\alpha^{\mathrm{r}}(\tau,\delta) = \sum N_i \tau^{t_i} \delta^{d_i} + \sum N_i \tau^{t_i} \delta^{d_i} \exp(-\delta^{e_i}) + \sum N_i \tau^{t_i} \delta^{d_i} \exp\left[-\eta_i(\delta-\varepsilon_i)^2 - \beta_i(\tau-\gamma_i)^2\right]. \tag{5}$$

In general, the number of terms and the values of the coefficients and exponents are determined through fitting of experimental data. The values of t_i should be greater than zero, and d_i and e_i should be integer values greater than zero. This work fitted the form to the selected experimental data through the use of the nonlinear fitting algorithm developed by Lemmon and Jacobsen (2005) and Lemmon et al. (2009). The fitting minimized the objective function F represented as

$$F^2 = \sum W_p F_p^2 + \sum W_\varrho F_\varrho^2 + \sum W_w F_w^2 + \cdots, \tag{6}$$

where F_X is the relative deviation in a calculated property X from an experimental value, and W_X is the weighting factor for F_X. For example, F_p, F_ϱ, and F_w are calculated as

$$F_p = \frac{p_{\mathrm{exp}} - p_{\mathrm{calc}}}{p_{\mathrm{exp}}}, \tag{7}$$

$$F_\varrho = \frac{p_{\mathrm{exp}} - p_{\mathrm{calc}}}{\varrho_{\mathrm{exp}}} \left(\frac{\partial \varrho}{\partial p}\right)_T, \tag{8}$$

and

$$F_w = \frac{w_{\mathrm{exp}} - w_{\mathrm{calc}}}{w_{\mathrm{exp}}}. \tag{9}$$

The pressure deviation F_p is calculated for $p\varrho T$ data in the vapor phase and critical region, and the density deviation F_ϱ is calculated for liquid phase $p\varrho T$ data. Deviations for other experimental data were added to the objective function in a similar manner as for the sound speed deviation F_w.

Each data point is individually weighted according to type, region, and uncertainty. In this work, typical values of W are about 1 for vapor pressures, 10 for $p\varrho T$ data in the liquid phase, 0.1 for $p\varrho T$ data in the vapor phase, and 100 for sound speeds in the vapor phase. During minimization of the objective function, various thermodynamic constraints were applied to ensure that the equation of state was well behaved in the vicinity of the critical point and would reliably extrapolate beyond the range of the experimental data. These constraints have been discussed and improved in the literature, e.g., Span and Wagner (1997), Lemmon and Jacobsen (2005), and Lemmon et al. (2009). For example,

the values of the first and second derivatives of pressure with respect to density were fitted so that their values would be zero at the critical temperature and density. This is confirmed in Figure 3. The second virial coefficient is obtained from the equation

$$B = \frac{1}{\varrho_c} \lim_{\delta \to 0} \left(\frac{\partial \alpha^r}{\partial \delta} \right)_\tau . \tag{10}$$

Below the Boyle temperature at which B is equal to zero, B should be negative and constantly decreasing. Above the Boyle temperature, B should increase to a maximum and then decrease to zero at very high temperatures. As shown in Figure 4, this is true of B values calculated from the equation.

Once the minimization finished, the number of significant digits in $\eta_i, \beta_i, \gamma_i$, and ε_i were rounded to four digits or less, and those of t_i were reduced to three digits or less, followed by refitting other coefficients and exponents with the same objective function. The final form of the residual part obtained in this work is

$$\alpha^r(\tau,\delta) = \sum_{i=1}^{5} N_i \tau^{t_i} \delta^{d_i} + \sum_{6}^{10} N_i \tau^{t_i} \delta^{d_i} \exp(-\delta^{e_i}) + \sum_{11}^{15} N_i \tau^{t_i} \delta^{d_i} \exp\left[-\eta_i (\delta - \varepsilon_i)^2 - \beta_i (\tau - \gamma_i)^2 \right], \tag{11}$$

where the coefficients and exponents are given in Table 4.

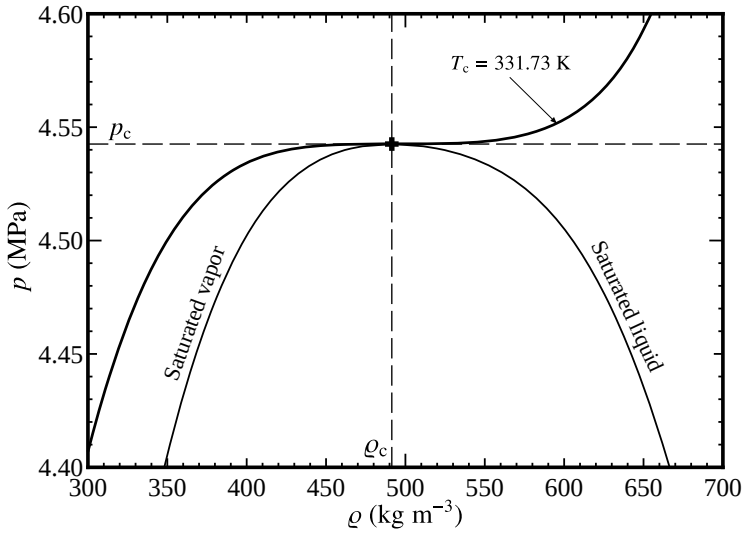

Figure 3: Saturation boundary and critical isotherm calculated from the equation of state: (+) Calculated critical point (491.43 kg m^{-3}, 4.5426 MPa)

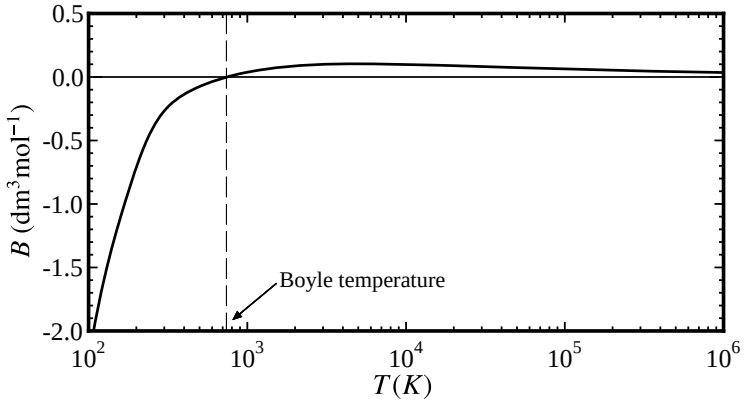

Figure 4: Second virial coefficient *B* calculated from the equation of state.

Table 4: Coefficients and exponents of Eq. (11)

i	N_i	t_i	d_i	e_i
1	0.044649519	1.	4	-
2	2.0208994	0.28	1	-
3	−2.6417598	0.782	1	-
4	−0.41197275	1.03	2	-
5	0.11153993	0.68	3	-
6	−1.3190495	1.64	1	2
7	−0.46464623	1.46	3	2
8	−0.040932167	2.23	2	1
9	0.26296637	1.2	2	2
10	−0.018089075	1.73	7	1

i	N_i	t_i	d_i	η_i	β_i	γ_i	ε_i
11	1.6070681	1.05	1	0.721	2.023	1.09	0.557
12	−0.73580167	1.13	1	1.261	1.705	1.2	0.353
13	−0.26768005	1.78	3	1.656	1.81	0.9	0.291
14	−0.28256773	0.96	2	0.804	3.1	1.123	0.736
15	−0.14045846	1.85	2	1.744	0.685	0.837	1.131

4. COMPARISONS TO EXPERIMENTAL DATA

Figure 5 shows deviations in experimental vapor pressures from calculated values with the equation of state. The equation was mainly fitted to the data by Higashi and Akasaka (2016). The maximum and average deviations in the Higashi and Akasaka data are 0.06 % and 0.03 %, respectively. The equation was roughly fitted to the simulation results by Raabe (2016), so that it has reasonable vapor pressures at temperatures below 300 K. The Raabe data are represented within 1.2 %, except the datum at 300 K. The data by Fukushima et al. (2015) and those by Kayukawa et al. (2015) are scattered, and they show systematic deviations from the equation of state.

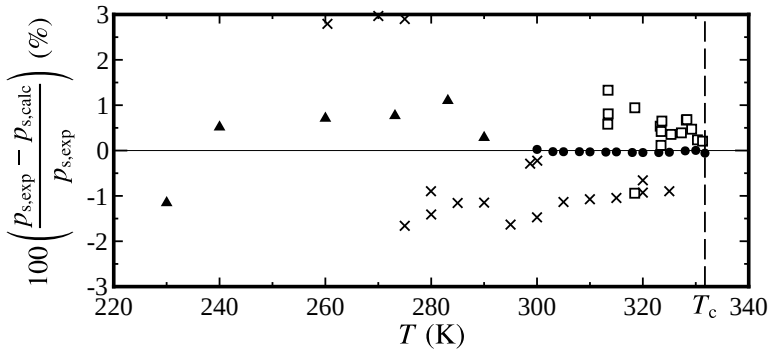

Figure 5: Deviations in experimental vapor pressures from calculated values with the equation of state: (□) Fukushima et al. (2015), (×) Kayukawa et al. (2015), (•) Higashi and Akasaka (2016), (▲) Raabe (2016)

The saturation boundary calculated from the equation of state is plotted on the T-ϱ diagram in Figure 6, along with experimental data for the saturated liquid and vapor densities. Figure 7 shows deviations in the experimental data of the saturated density from the equation. The equation was fitted to the data by Fukushima et al. (2015) and those by Higashi and Akasaka (2016). Due to high uncertainties, some data near the critical point were not used in the fitting, but Figures 6 and 7 show that all experimental data are well represented from 230 K to the critical temperature. The AADs in the Fukushima data are 0.24 % below 324 K and 1.56 % at higher temperatures. The Higashi and Akasaka data are represented with an AAD of 0.53 %. The rectilinear diameter, a mean value of the saturated liquid and vapor densities, is also shown in Figure 6, and is nearly straight from 240 K to the critical point. This means that the saturated liquid and vapor densities calculated from the equation are reliable over a large temperature range.

Figure 8 shows deviations in experimental densities from the equation of state. The fitting used the data in the liquid and vapor phases by Higashi and Akasaka (2016), the gas phase data below 2 MPa by Kayukawa et al. (2015), and the liquid phase data below 280 K by Kayukawa (2016). The data by Fukushima et al. (2015) were not used in the fitting due to their lower reliability. The Higashi and Akasaka data are represented within 0.76 % with an AAD of 0.15 %. Although the gas phase data by Kayukawa et al. (2015) show systematic negative deviations, the AAD in the data is 0.58 %, and is similar to the experimental uncertainty claimed by the author. Inconsistency is observed in the

liquid phase data by Kayukawa (2016) with those by Higashi and Akasaka (2016) below 900 kg m^{-3}, and therefore only higher densities below 280 K were selected from the Kayukawa data for fitting. The AAD in the selected liquid densities is 0.11 %.

Figure 9 shows deviations in the vapor phase sound speeds by Kano et al. (2016). Almost all data points are represented within 0.1 %, and the AAD in the data is 0.03 %.

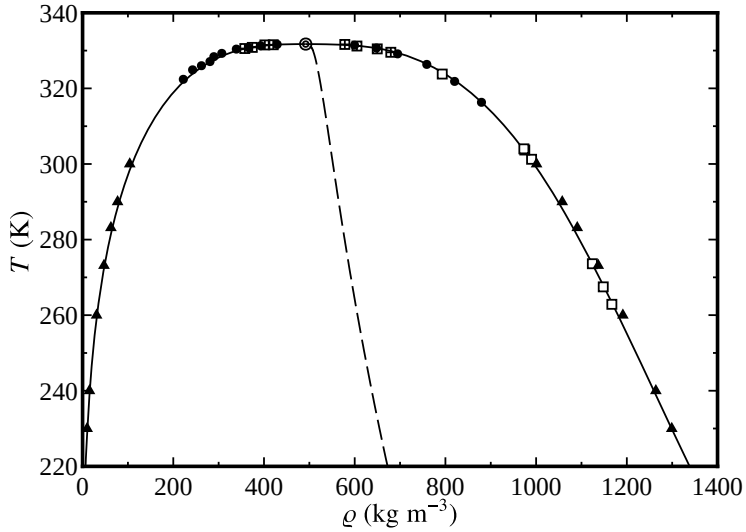

Figure 6: Saturation boundary calculated from the equation of state and experimental data for the saturated liquid and vapor densities: (□, ⊞) Fukushima et al. (2015), (•) Higashi and Akasaka (2016), (▲) Raabe (2016), (◎) Critical point calculated form the equation of state (491.43 kg m^{-3}, 331.73 K). The dashed line shows the rectilinear diameter $(\varrho' + \varrho'')/2$.

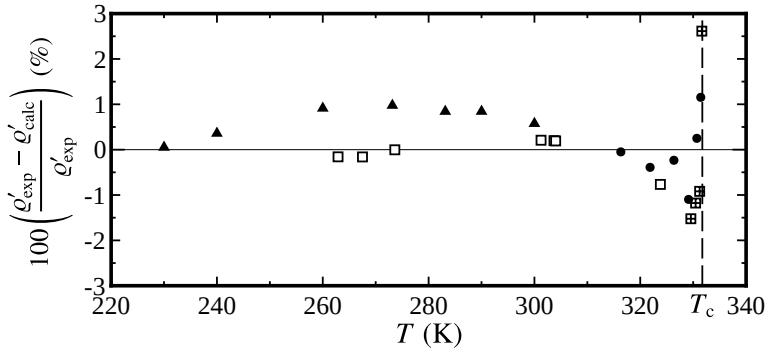

Figure 7: Deviations in experimental saturated liquid density data from calculated values with the equation of state: (□, ⊞) Fukushima et al. (2015), (•) Higashi and Akasaka (2016), (▲) Raabe (2016)

5. EXTRAPOLATION BEHAVIOR

In order to verify the behavior of the equation of state in regions away from the experimental data, the following four characteristic curves are useful: the ideal curve, the Boyle curve, the Joule-Thomson inversion curve, and the Joule inversion curve. These characteristic curves obtained from the equation of state are shown in Figure 10. The reasonable shapes of these curves clarify qualitatively correct extrapolation behavior of the equation extending to extremely high pressures and temperatures. Moreover, plots of temperature versus isobaric heat capacity, sound speed, and the phase identification parameter defined by Venkatarathnam and Oellrich (2011) are shown in Figures 11, 12, and 13, respectively. These plots indicate that the equation exhibits correct behavior over all temperatures and pressures within the range of validity, and shows reasonable extrapolation behavior at higher temperatures and pressures.

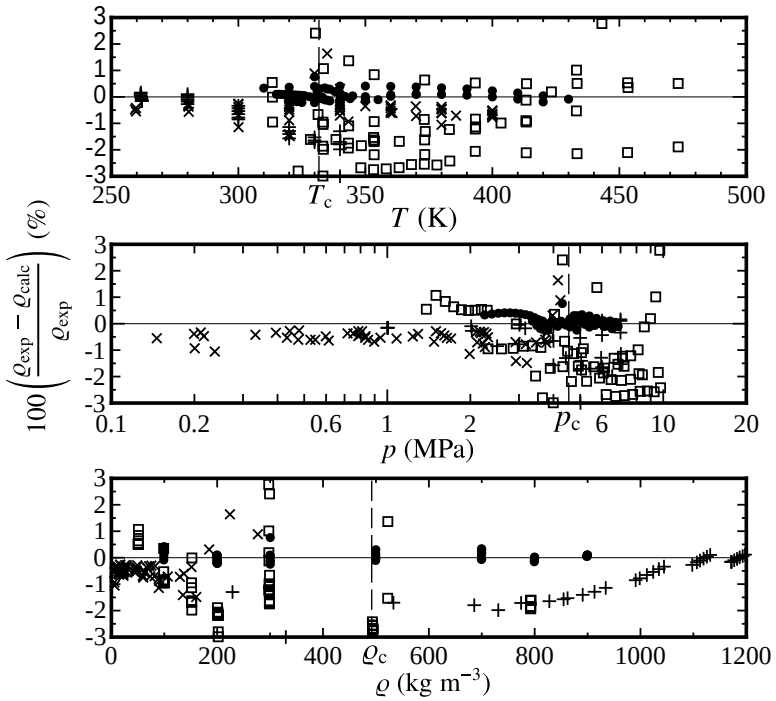

Figure 8: Deviations in experimental densities from calculated values with the equation of state: (□) Fukushima et al. (2015), (×) Kayukawa et al. (2015), (•) Higashi and Akasaka (2016), (+) Kayukawa (2016).

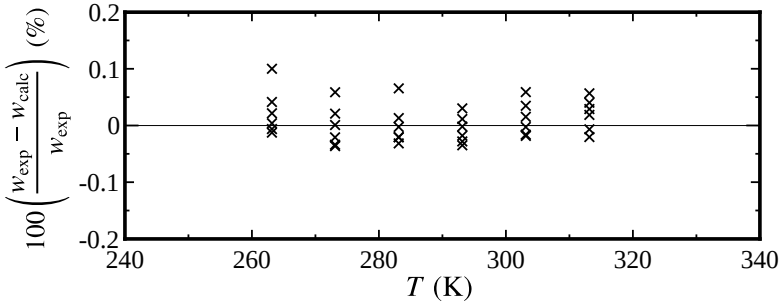

Figure 9: Deviations in experimental data for the vapor-phase sound speed from calculated values with the equation of state: (×) Kano et al. (2016)

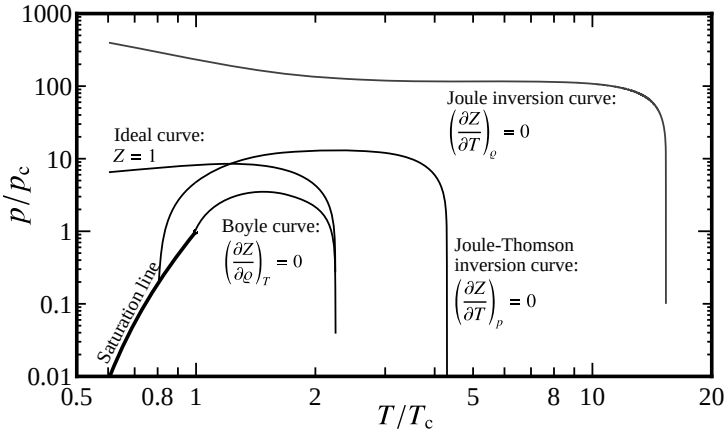

Figure 10: Four characteristic curves of the equation of state as a function of reduced temperature and reduced pressure

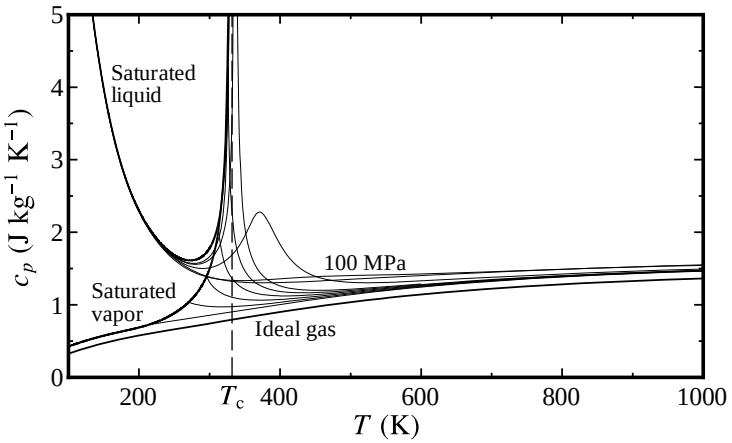

Figure 11: Plot of temperature versus isobaric heat capacity obtained from the equation of state along isobars at (100, 50, 10, 5, 4, 3, 2, 1, 0.1) MPa and 0 MPa (ideal gas).

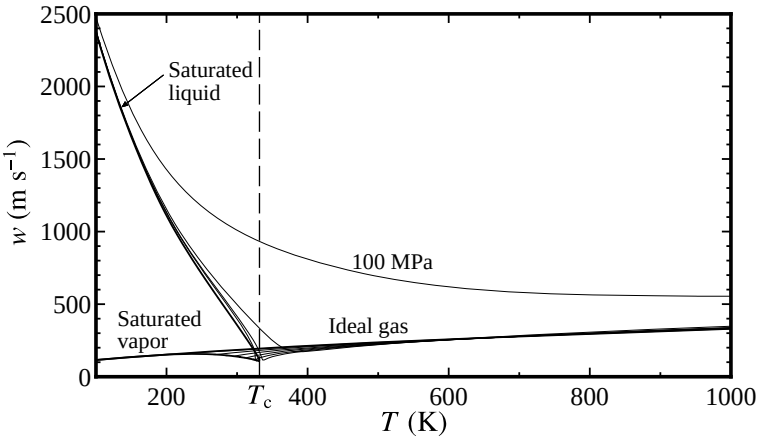

Figure 12: Plot of temperature versus sound speed obtained from the equation of state along isobars at (100, 50, 10, 5, 4, 3, 2, 1, 0.1) MPa and 0 MPa (ideal gas).

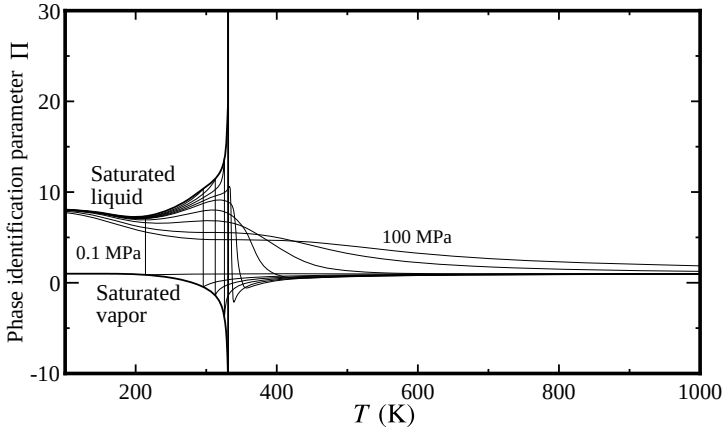

Figure 13: Plot of temperature versus phase identification parameter along isobars at (100, 50, 20, 6, 5, 4, 3, 2, 1, and 0.1) MPa

6. CONCLUSIONS

The equation of state for R-1123 was successfully fitted for the Helmholtz energy as the fundamental property. The equation is valid for temperatures from 250 K to 480 K and for pressures up to 10 MPa. Comparisons to experimental data demonstrated that typical uncertainties in calculated properties are 0.1 % for vapor pressures, 0.2 % for liquid densities, and 1 % for vapor densities, except in the critical region where larger deviations up to 2 % are sometimes observed in densities. Deviations in calculated vapor pressures are larger at temperatures below 300 K. Several plots of constant-property lines showed that the equation exhibits correct behavior over all temperatures and pressures within the range of validity, and that it shows reasonable extrapolation behavior at higher temperatures and pressures.

We have already started the next work on formulating a mixture model for R-32/1123 mixtures. This will be presented at the 11th Asian Thermophysical Properties Conference (October 2016, Yokohama, Japan).

REFERENCES

Fukushima, M., Hayamizu, H., Hashimoto, M. (2015). Thermodynamic properties of low-GWP alternative refrigerants, *Proceedings of the 24th IIR International Congress of Refrigeration*, Yokohama, Japan.

Higashi, Y., & Akasaka, R. (2016). Measurements of thermodynamic properties for R1123 and R1123+R32 mixture, *Proceedings of the 16th International Refrigeration and Air Conditioning Conference at Purdue* (Paper ID 283), West Lafayette, IN, USA.

Kano, Y., Kayukawa, Y., Fujita, Y., Hashimoto, M., Fukushima, M. (2016). Speed of sound measurement for R1123 in the gas phase to derive the ideal gas heat capacity, *Proceedings of the 8th Asian Conference on Refrigeration and Air Conditioning*, Taipei, Taiwan.

Kayukawa, Y. (2016). unpublished data.

Kayukawa, Y., Kano, Y., Fujita, Y., Hashimoto, M., Fukushima, M. (2015). Measurements for vapor pressures and PVT properties for low-GWP refrigerant, HFO1123, by a magnetic levitation densimeter (in Japanese), *Proceedings of the JSRAE 2015 Annual Conference*, Tokyo, Japan.

Joback, K. G., & Reid, R. C. (1987). Estimation of pure-component properties from group-contributions, *Chem. Eng. Comm.*, 57(1-6), 233–243.

Lemmon, E. W., & Jacobnsen, R. T. (2005). A new functional form and new fitting techniques for equations of state with application to pentafluoroethane (HFC-125), *J. Phys. Chem. Ref. Data*, 34(1), 69–108.

Lemmon, E. W., McLinden, M. O., Wagner, W. (2009). Thermodynamic properties of propane. III. A reference equation of state for temperatures from the melting line to 650 K and pressures up to 1000 MPa, *J. Chem. Eng. Data* 54(12), 3141–3180.

Mohr, P. J., Taylor, B. N., Newell, D. B. (2012). CODATA Recommended Values of the Fundamental Physical Constants: 2010, *Rev. Mod. Phys.*, 84(4), 1527–1605.

Raabe, G. (2016). Molecular simulation studies in HFO working fluids and their blends, to be published in *Science and Technology for the Built Environment.*

Span, R., & Wagner, W. (1997). On the extrapolation behavior of empirical equations of state, *Int. J. Thermophys.*, 18(6), 1415–1443.

Venkatarathnam, G. & Oellrich, L.R. (2011). Identification of the phase of a fluid using partial derivatives of pressure, volume, and temperature without reference to saturation properties: Applications in phase equilibria calculations, *Fluid Phase Equilib.*, 301, 225–233.